

Multimodal Cancer Modeling in the Age of Foundation Model Embeddings

Steven Song*

*Center for Translational Data Science
Department of Computer Science
Medical Scientist Training Program
University of Chicago, Chicago IL, USA*

SONGS1@UCHICAGO.EDU

Morgan Borjigin-Wang*†

*Department of Computer Science
Brown University, Providence RI, USA*

MBWANG@BROWN.EDU

Irene Madejski

*Center for Translational Data Science
Department of Computer Science
University of Chicago, Chicago IL, USA*

IMADEJSKI@UCHICAGO.EDU

Robert L. Grossman

*Center for Translational Data Science
Department of Computer Science
Section of Biomedical Data Science, Department of Medicine
University of Chicago, Chicago IL, USA*

RGROSSMAN1@UCHICAGO.EDU

Abstract

The Cancer Genome Atlas (TCGA) has enabled novel discoveries and served as a large-scale reference dataset in cancer through its harmonized genomics, clinical, and imaging data. Numerous prior studies have developed bespoke deep learning models over TCGA for tasks such as cancer survival prediction. A modern paradigm in biomedical deep learning is the development of foundation models (FMs) to derive feature embeddings agnostic to a specific modeling task. Biomedical text especially has seen growing development of FMs. While TCGA contains free-text data as pathology reports, these have been historically underutilized. Here, we investigate the ability to train classical machine learning models over multimodal, zero-shot FM embeddings of cancer data. We demonstrate the ease and additive effect of multimodal fusion, outperforming unimodal models. Further, we show the benefit of including pathology report text and rigorously evaluate the effect of model-based text summarization and hallucination. Overall, we propose an embedding-centric approach to multimodal cancer modeling.

Keywords: Multimodal Cancer Data, Foundation Models, Biomedical Embeddings, TCGA, Pathology Report Summarization

Data and Code Availability TCGA data is publicly available through the GDC API. Extracted pathology reports from Mendely, DOI: 10.17632/hyg5xkznp1. Precomputed embeddings of WSIs from HuggingFace: MahmoodLab/UNI2-h-features. Our source code is available from: <https://github.com/StevenSong/multimodal-cancer-modeling>.

Institutional Review Board (IRB) This research does not require IRB approval.

1. Introduction

The Cancer Genome Atlas (TCGA) has been the premier cancer research resource for nearly two decades (Tomczak et al., 2015). Throughout its history, its harmonized data (Heath et al., 2021) has enabled novel discoveries through its multitudes of molecular genetic data (Zhang et al., 2021), histopathological images, and clinical descriptors for over 11 thousand cases across 33 cancer types. There have been nu-

* These authors contributed equally

† Work performed as a research volunteer at CTDS.

merous studies which develop deep learning methods using TCGA (Sartori et al., 2025) for various tasks, however TCGA cancer survival has been particularly well studied (Abbasi et al., 2024; Arjmand et al., 2022; Liu et al., 2018).

There have been numerous studies to date that have trained bespoke models to predict patient survival from TCGA. These models have covered a wide range in the specific cancer types studied, the data modalities used as predictive features, and the model types trained. Some have leveraged histology images (Wulczyn et al., 2020; Yang et al., 2025) or RNA sequencing (RNaseq) (Ching et al., 2018; Huang et al., 2020; Qiu et al., 2020; Nayshool et al., 2022) alone, while others have explored varying degrees of multimodal integration (Chaudhary et al., 2018; Zhan et al., 2019; Hao et al., 2019; Ramirez et al., 2021; Malik et al., 2021; Redekar et al., 2022; Sun and Chen, 2023; Fan et al., 2023; Hao et al., 2023). Most recent papers focus on training task-specific deep-learning models (Ching et al., 2018; Hao et al., 2019; Huang et al., 2020; Wulczyn et al., 2020; Qiu et al., 2020; Ramirez et al., 2021; Malik et al., 2021; Sun and Chen, 2023; Fan et al., 2023; Hao et al., 2023; Yang et al., 2025) and some apply simpler machine learning models (Zhan et al., 2019; Nayshool et al., 2022; Redekar et al., 2022), however few explore the synergy of combining deep learning with simpler statistical, machine learning models (Chaudhary et al., 2018).

A modern paradigm in biomedical deep learning is the development of foundation models (FMs) to derive meaningful feature embeddings (Bommasani et al., 2021). These FMs are typically trained over large corpora of data using self-supervision to improve generalization of embeddings to downstream tasks. Biomedical text especially has seen growing development of FM large language models (LLMs) (Singhal et al., 2023; Thirunavukarasu et al., 2023). While many LLMs have been adapted towards the biomedical domain using research text from PubMed and PubMed Central (Gu et al., 2021; Bolton et al., 2024; Labrak et al., 2024), more specific pathology-report text FMs have also been developed as vision-language models (Lu et al., 2024; Xiang et al., 2025).

While TCGA contains free-text data as pathology reports, these have been historically underutilized. This may in part be due to the difficulty of working with the raw data format of these reports as scanned PDFs. With the current interest in applications of LLMs to biomedical domains, a recent effort by Kefeli and Tatonetti (2024a) used optical character recog-

nition to extract the text from all available PDFs of TCGA. To the best of our knowledge, only one other work has explored the application of TCGA reports towards survival modeling (Xiang et al., 2025) and differs from our approach (see Section 4).

Here, we investigate the combination of simple machine learning models with modern FMs (Figure 1) for predicting cancer survival using multimodal data from TCGA.

Our main contributions are:

- **Quantification of pan-cancer survival prediction using rich embeddings with small models.** We contemporize survival modeling for TCGA, the premier cancer research resource, using zero-shot, foundation model-derived embeddings combined with small models. Despite advanced deep learning methods, survival models over FM embeddings of single data modalities do not do substantially better than survival models over 5 tabular clinical features (see Section 3.2).
- **Simple framework for multimodal fusion of many data modalities that improves cancer survival prediction.** We introduce a modular framework to do late-fusion of unimodal models, that is extensible to variable data modalities and embedding methods. Using our approach, we demonstrate that cancer data modalities are additive and non-redundant, including tabular clinical features (see Section 3.3).
- **Analysis on the effect of clinical text summarization and model hallucination on cancer modeling.** We develop a method for automatic pathology report summarization and propose an approach to rigorously evaluate the effect of LLM hallucinations during summarization. We demonstrate that summarizing pathology report text improves survival prediction and that LLM hallucinations do not impact survival predictions over their derived embeddings (see Sections 3.4 and 3.5).

2. Methods

2.1. Data and Experimental Setup

We use TCGA patient cases which have available and valid survival data, pathology reports, tumor diagnostic slides, and tumor RNA-seq gene expression.

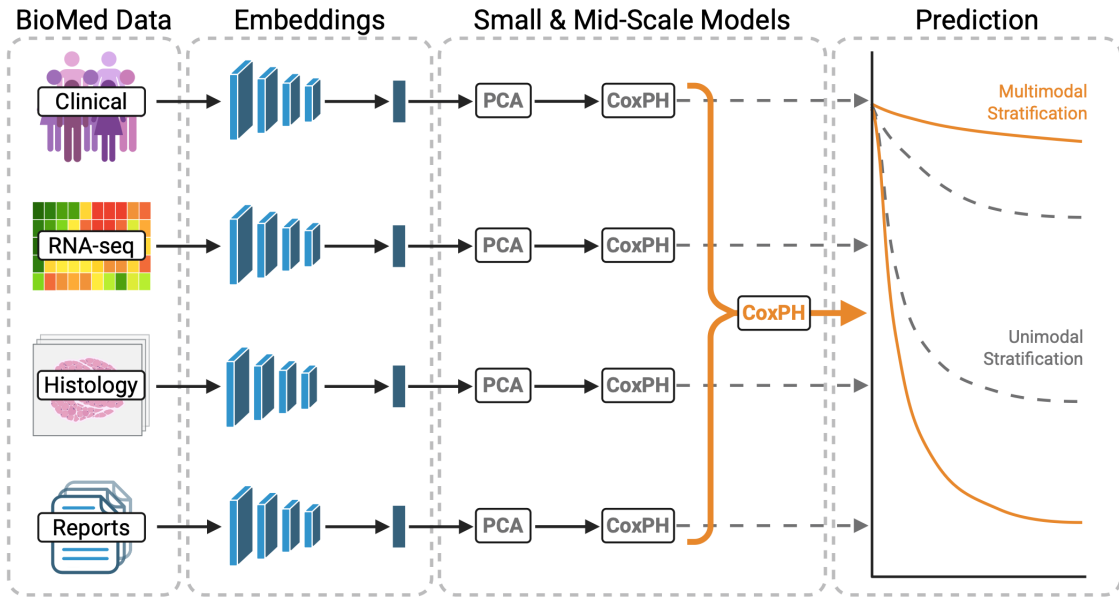


Figure 1: Multimodal cancer modeling is vastly simplified in the age of foundation models. Simple ensembles of small, classical models over zero-shot FM embeddings improve pan-cancer survival risk stratification. Embedding methods are modular, allowing for simple experimentation and orchestration.

For pathology reports, we use text extracted by [Kefeli and Tatonetti \(2024a\)](#). For computational efficiency, we additionally rely on precomputed UNI2 embeddings of diagnostic slides by Chen et al. ([Chen et al., 2024](#)). Given these requirements, we first filter TCGA cases by the availability of pathology report, diagnostic slide, then RNA-seq data. We download the extracted text from Mendeley ([Kefeli and Tatonetti, 2024b](#)), precomputed UNI2 embeddings of diagnostic slides from HuggingFace ([Chen et al., 2025](#)), and RNA-seq data using the Genomic Data Commons (GDC) API ([Heath et al., 2021](#)). We ensure that the RNA-seq and diagnostic slides are derived from tumor samples.

We then select cases with valid demographic and survival data, again downloaded using the GDC API. Specifically, we compute survival as the time between the patient’s age at primary diagnosis and the patient’s age at last followup or death. We additionally require non-missing patient sex. Given the final set of cases, we split our dataset for 5-fold cross-validation. We stratify by patient age, sex, race, ethnicity, mortality, and cancer type. To stratify by age, we discretize age into 20-year age bins, i.e. [0-20), [20-40),

[40-60), [60-80), and 80+. For race and ethnicity, missing values are replaced with “Not Reported”. We one-hot encode demographic features (binned age, sex, race, ethnicity) and cancer type (TCGA project) for stratification and downstream modeling, resulting in 17 and 32 features, respectively.

2.2. Automated Report Summarization and Manual Correction

While the extracted pathology reports ([Kefeli and Tatonetti, 2024a](#)) are a rich source of information, they present multiple challenges. As the source reports are scanned documents of varying quality, the OCR extraction process can result in typos and loss of structured text. Additionally, the reports are often long with repeated information or information potentially irrelevant for cancer prognosis (e.g. incidental findings on histology).

To address these challenges, we experiment with having an LLM summarize the pathology reports to help focus relevant information, correct typos, and reduce report length. We choose Llama-3.1-8B-Instruct ([Grattafiori et al., 2024](#)) as the summarization model for its strong instruction following capabilities. We

use vLLM (Kwon et al., 2023) for inference with set seed, greedy decoding, temperature 0, and max tokens 1,024. Our prompt is presented in Table 10.

As we experiment with model generated summaries of pathology reports, we test the effect of model hallucinations (Huang et al., 2025) in the generated summaries and their downstream effects on survival modeling. To that end, we manually review model generated summaries for 40 randomly selected cases contained within a single test split. We randomly select these cases while preserving the overall prevalence of observed mortality. After review and manual correction (as needed) of the sampled summaries, we embed the corrected summaries using BioMistral and apply the survival model trained over BioMistral embeddings of summaries from the corresponding train split. We evaluate risk stratification over these sampled cases. Further details of our manual correction method are in Appendix A.

2.3. Foundation Model Embeddings

We use several foundation models in our experiments. For all FMs, we use the models as-is with no further training or fine-tuning. To prevent data leakage, we ensure that the FMs we use have not been trained over TCGA. Specifically, we experiment with UNI2-h (Chen et al., 2024) for diagnostic slides, BulkRNABert (Gélard et al., 2025) or UCE (Rosen et al., 2023) for gene expression data, and BioMistral-7B (Labrak et al., 2024) or Mistral-7B-Instruct-v0.1 (Jiang et al., 2023) for pathology reports. Further details on these models is presented in Appendix B.

As survival is defined at the patient-level, we aggregate patient embeddings from multiple samples of the same modality into a single embedding per patient per modality. This is most relevant for RNA-seq and diagnostic slides as a patient may have multiple samples for these modalities. We use simple averaging of embeddings to derive our patient-level embeddings. Model embedding dimensionality shown in Table 12.

2.4. Unimodal and Multimodal Survival Modeling and Evaluation

Given patient-level, modality-specific embeddings, we adopt a simple pipeline for unimodal survival modeling. For a given train-test split, we z-score standardize all embeddings using per-feature mean and standard deviation derived from the training split. We next derive a Principal Component Analysis (PCA) (Pearson, 1901) dimensionality reduction

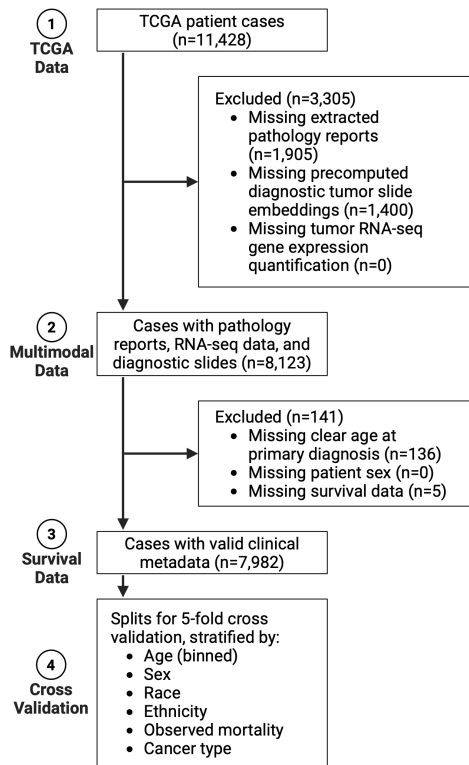


Figure 2: Eight thousand patient cases spanning 32 cancer types with survival data, pathology reports, diagnostic slides, and gene expression quantification.

over the standardized embeddings from the training split and apply to all standardized embeddings. We use dimensionality reduction to prevent overfitting and improve computational tractability (see Table 13 and Appendix E for results and discussion on using full embeddings). As PCA is an efficient transformation that is insensitive to hyperparameter choices (as in t-SNE or UMAP), we specifically use the implementation of PCA from sklearn (Pedregosa et al., 2011) with a set seed. We experiment with varying PCA dimensions, doubling from 4 to 256. For demographic or cancer type modalities, features are one-hot encoded so we do not apply standardization or PCA transformation. We then fit a Cox Proportional Hazards (CoxPH) (Cox, 1972) model to the PCA reduced embeddings (or the one-hot encoded features for demographic or cancer type modalities) of the train split. We use the implementation of CoxPH

Table 1: Foundation model derived embeddings predict cancer survival. Average cross-validated C-index of CoxPH models trained over unimodal embeddings across varying PCA reductions. Demo: demographics; Canc: cancer type; Expr: BulkRNABert embedded RNA-seq; Hist: UNI2 embedded histology; Text: BioMistral embedded summarized pathology reports. *Not reduced with PCA.

Modality	PCA Dimension							
	4	8	16	32	64	128	256	N/A
Demo*	-	-	-	-	-	-	-	0.630
Canc*	-	-	-	-	-	-	-	0.737
Expr	0.626	0.650	0.702	0.742	0.749	0.753	0.750	-
Hist	0.596	0.631	0.669	0.714	0.733	0.748	0.754	-
Text	0.565	0.610	0.690	0.725	0.745	0.751	0.752	-

models from `sksurv` (Pölsterl, 2020) with $\alpha = 0.1$ for ridge regression penalty. Using the trained unimodal model, we predict risk scores for both the train and test splits for further modeling and evaluation.

We do late multimodal fusion using the predicted unimodal risk scores as input to the multimodal model. Given a set of modalities we aim to fuse, we concatenate the predicted risk scores from each modality as input features. We z-score standardize each feature using the mean and standard deviation derived over the training split. We fit a CoxPH model over the concatenated, standardized, unimodal risk scores. Such a model can be interpreted as modeling the unimodal risk (further discussed in Section 3.3). Using the trained multimodal model, we predict risk scores for the test split for evaluation. We repeat this multimodal fusion procedure over all combinations of demographic, cancer type, histology, expression, and text modalities. Notably, we do not consider alternate embedding methods as separate modalities; for example BioMistral embeddings of unsummarized and summarized reports are both text embeddings. Instead, we consider multimodal combinations with these alternate embedding strategies independently.

We evaluate the resulting models using 5-fold cross-validated concordance index (C-index) (Harrell et al., 1982), mean cumulative/dynamic area under the receiver operating characteristic curve (mean $AUC^{C,D}$, where larger is better) (Lambert and Chevret, 2016), integrated Brier score (IBS, where smaller is better) (Brier, 1950), or risk stratified Kaplan-Meier (Kaplan and Meier, 1958) survival curves. Precise details on our evaluation method are provided in Appendix C.

3. Results

3.1. Multimodal data across 32 cancers

We assemble a dataset of 7,982 patient cases for our study (Figure 2). These cases span 32 of the 33 cancer types in TCGA. We select cases that have available and valid data for survival analysis, pre-extracted pathology reports by Kefeli and Tatonelli (Kefeli and Tatonetti, 2024a), precomputed tumor diagnostic slide embeddings by Chen et al. (Chen et al., 2024), and tumor RNA-seq gene expression data.

For our experiments, we split the dataset into 5 stratified cross-validation folds that are shared across all experiments. Descriptive features of our dataset and splits are provided in Tables 15 and 16. While we stratify by cancer type and observed mortality, we do not stratify by survival duration. On average, overall survival time is comparable across splits, however per-cancer type subsets contained within each split may have too few observed mortalities for survival modeling (Table 16). See Appendix C for details on the limitations this presents for evaluating model performance within given cancer types.

3.2. Unimodal FM embeddings predict cancer survival

We fit small, linear CoxPH survival models over unimodal data and attain a peak mean cross-validated C-index of approximately 0.75 over single modalities (Table 1). For categorical demographic features or cancer type, we do no dimensionality reduction. As compared to the mixture of models over both clinical tabular features (Canc-Demo C-index = 0.747, Table 2), CoxPH models fit over demographic features

Table 2: Mixing survival models of clinical features with FM-based survival models improves survival prediction. For the best combination of each number of modality combinations, average cross-validated C-index of multimodal CoxPH models trained over predicted risk scores from unimodal CoxPH models across varying PCA reductions. Demo: demographics; Canc: cancer type; Expr: BulkRNA-Bert embedded RNA-seq; Hist: UNI2 embedded histology; Text: BioMistral embedded summarized pathology reports. *Not reduced with PCA.

Modality	PCA Dimension							
	4	8	16	32	64	128	256	N/A
Canc*-Demo*	-	-	-	-	-	-	-	0.747
Hist-Text	0.606	0.662	0.705	0.746	0.767	0.777	0.780	-
Expr-Hist-Text	0.644	0.682	0.727	0.765	0.780	0.786	0.788	-
Demo*-Expr-Hist-Text	0.680	0.717	0.748	0.776	0.788	0.794	0.795	-
Canc*-Demo*-Expr-Hist-Text	0.749	0.752	0.760	0.777	0.788	0.793	0.793	-

or cancer type alone achieve slightly lower C-index (0.630 and 0.737, respectively).

For FM-derived embeddings (expression, histology, and text), we tested varying PCA sizes for dimensionality reduction. We observe a general trend of increasing C-index with increasing PCA dimensions, which plateaus around PCA to 256 dimensions. These findings are recapitulated using additional metrics of mean $AUC^{C,D}$ and IBS (Tables 5 and 4, respectively). Based on this observation, we report further results using PCA transformation of these embeddings to 256 dimensions.

With the same unimodal survival models, we evaluate their survival prediction performance across individual cancer types (Tables 3 and 17). We do not evaluate per-cancer survival based on cancer type as the input features would not differ within a cancer subset. We not only find that survival modeling performance of unimodal models varies across cancer types, we also observe that no single modality generally outperforms the other modalities. For example, among unimodal models, demographic-based modeling was most predictive of thyroid carcinoma (THCA) survival (C-index = 0.885), while the same was true for text report-based modeling of endometrial carcinoma (UCEC) survival (C-index = 0.723).

3.3. Multimodal fusion improves cancer modeling and survival prediction

While unimodal models were able to achieve a peak C-index of approximately 0.75, we find that all multimodal fusion models are able to surpass unimodal re-

sults at their corresponding PCA reductions (Tables 2 and 6). We again observe a plateau of survival model performance at PCA = 256 and thus report results using this dimensionality reduction for embeddings. Importantly, each modality is independently modeled at a given PCA dimensionality before the predicted unimodal risk scores are subsequently used as input features to the multimodal fusion model (Section 2.4).

Using this simple, late multimodal fusion technique, we find that fusion of expression with histology data, expression with report data, and histology with report data result in mean cross-validated C-index = 0.774, 0.778, and 0.780, respectively (Table 6). Fusion of all three of expression, histology, and reports results in the best embedding-based performance of C-index = 0.788. Survival modeling with these embedding-based modalities are not only additive, but also can be further enhanced with clinical features, such as demographics, achieving our greatest C-index = 0.795 (Table 2). The additive effect of multimodal fusion is further observed in both mean $AUC^{C,D}$ and IBS (Tables 5 and 4, respectively). Importantly, these modalities are encoding information beyond simply cancer type, as any combination of modalities with cancer type improves upon the results of using cancer type alone (Table 7).

Additionally, as before, the ability to model survival within each cancer type further substantiates this claim, as the unimodal model based on cancer type cannot predict survival within a single cancer type. When examining multimodal model performance subset by cancer type in Tables

Table 3: Multimodal fusion improves survival prediction within the 8 most prevalent cancer types in the TCGA. Average cross-validated C-index of models using PCA to 256 dimensions for all foundation model derived embeddings. Multimodal model used fusion of all unimodal modalities.

Modality	Cancer Type (TCGA Project)							
	BRCA	KIRC	UCEC	THCA	LGG	HNSC	LUSC	LUAD
Demographics	0.637	0.600	0.593	0.885	0.727	0.525	0.542	0.530
RNA-seq	0.573	0.673	0.643	0.619	0.790	0.560	0.579	0.620
Histology	0.648	0.685	0.703	0.749	0.753	0.636	0.598	0.617
Text	0.641	0.698	0.723	0.619	0.716	0.582	0.556	0.645
Multimodal	0.720	0.752	0.758	0.787	0.840	0.650	0.626	0.687

3 and 17, we find that multimodal fusion consistently performs better than any other modality within a given cancer type for the most prevalent cancer types (see Appendix C for additional details on evaluations within cancer types). This is in contrast to the unimodal models where the best unimodal model differs depending on the cancer.

Interpretability. Under our framework for multimodal fusion, a natural interpretation of the multimodal model arises. As the input to the multimodal CoxPH model are z-score normalized unimodal risk scores, the hazard ratios of the trained multimodal model can be interpreted relative to the standard deviations of the unimodal predicted risks. In other words, the hazard ratio for a given modality is the relative risk of death for a one standard deviation increase in that modality’s unimodal predicted risk. Table 8 presents the hazard ratios of the 5-modality model (using unimodal models over PCA = 256 for high-dimensional embeddings). We find that the high-dimensional inputs confer greater relative risk, recapitulating our observations that these modalities are informative beyond tabular features.

3.4. Pathology report summarization focuses cancer information

One of our key findings is that LLM summarization of pathology reports drastically improves survival prediction. Specifically, we zero-shot prompt Llama-3.1-8B-Instruct to summarize pathology reports with a focus on microscopic descriptions, test results, diagnoses, and clinical history. See Section 2.2 for more details on our summarization method.

Using Llama generated summaries, we embed the summarized reports using BioMistral. As compared with BioMistral embeddings of the original, unsummarized reports, we find that the summarized reports are able to better predict survival (C-index = 0.752 for summarized vs C-index = 0.694 for unsummarized). Using the predicted risk scores, we stratify the study cohort into low and high risk groups and observe that summarized reports result in enhanced risk stratification (Figure 3).

Not only does summarization reduce the token length of the original report, it also corrects typographical errors that may result from text extraction from the source scanned PDFs of these reports. In addition, prompting the summarization to focus on certain aspects of the report may better extract information most relevant to survival prediction. With these effects in combination, we observe that embeddings of summarization outperforms embeddings of the original report across the 8 most prevalent cancer types (Table 9).

3.5. Hallucination correction does not impact cancer risk stratification

While we empirically find that summarization improves survival prediction, hallucinations are an important consideration when using LLM generated text. To test whether factually incorrect information in the generated summaries impact downstream survival modeling, we manually correct generated summaries for these hallucinations.

To that end, we develop and share a lightweight tool to facilitate comparison of original and summarized reports. A screenshot of the tool is pre-

sented in Figure 7. Using this utility, we review 40 randomly sampled reports contained within a single cross-validation fold. We ultimately apply minor corrections to 24 of 40 reports. See Appendix A for additional details, such as methodology and categorization of manual corrections.

After manual correction, we re-embed the corrected summaries and do survival prediction using the same CoxPH model trained on uncorrected summarized embeddings. For the subset of corrected reports, we compare against the corresponding uncorrected summaries (Figure 4). We empirically find that risk stratification of the sampled subset does not change based on correction of hallucinations. This may be because the corrections on average are qualitatively minor compared to the majority of the summary (Table 11). We hypothesize that the salient information for predicting cancer survival, such as cancer severity, extent of invasion or metastasis, remained unchanged, though further work is needed.

3.6. Impact of domain specificity on cancer modeling and survival prediction

Our final set of experiments were ablations to test the impact of foundation model domain specificity for downstream embedding-based modeling. For space, extended results are presented in Appendix D. In brief, domain adaptation is particularly important for data modality specificity (BulkRNABert is notably better than UCE for RNA-seq data, Figure 5), however specificity to biomedical text (BioMistral vs Mistral) matters less than summarization (Figure 6).

4. Discussion

Our study demonstrates the ease with which multimodal cancer modeling is accomplished in the age of foundation models. We show that zero-shot embeddings of unseen data can serve as the basis for prediction of cancer prognosis. We emphasize that our final survival models are combinations of classical CoxPH models with FM derived embeddings and five tabular, clinical features. The synergy between feature-rich embeddings and simple linear models enables prediction of complex biological tasks (Ahlmann-Eltze et al., 2024). This powerful paradigm in modern deep learning is additionally beneficial in medical settings where data privacy is a chief concern and model tuning can lead to memorization of small datasets of protected patient data (Moor et al., 2023; Kaissis et al.,

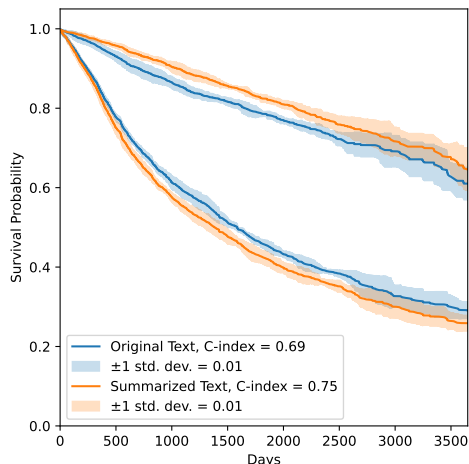


Figure 3: Summarization of pathology reports improves survival model risk stratification over unimodal text embeddings. Embeddings derived with BioMistral. Reports summarized with Llama-3.1-8B-Instruct. Averaged risk stratification from 5-fold cross-validation.

2020; Khalid et al., 2023; Torkzadehmahani et al., 2022). In our results, we rely on FMs trained over deidentified and often public data; we do not train any deep learning models. It is important to note that this low-resource approach applies to settings that do not have the compute infrastructure for supervised training of bespoke deep learning models.

Importantly, we compare survival models over more complex modalities against survival models over basic clinical tabular features spanning four demographic features (age, sex, race, ethnicity) and cancer type. We observe that unimodal survival predictions over FM embeddings of expression, histology, or test data are no better than the combination of demographics and cancer type. This is a critical baseline to contextualize the relative benefit of more complex methods over standard, classical models. Indeed, survival rates vary by cancer type as a complex interaction of biological and socioeconomic factors (Siegel et al., 2025) and thus, such tabular features may simply be correlative. Additionally, survival prediction within a given cancer type cannot be predicted by the cancer type itself. For these reasons, unimodal models over FM embeddings may still have utility.

To that end, the results from our simple framework for multimodal survival modeling additionally show that extracted information from single modalities is additive and that multimodal fusion is able to achieve impressive prediction accuracy. This additive effect may be explained by the varying unimodal results for per-cancer survival modeling, as we find that no single unimodal model excels across all cancer type subsets in TCGA. Conversely, our multimodal model excels across a majority of highly prevalent cancer types. Further, in sequential addition of modalities, we find that FM embeddings for these modalities are non-redundant (contrary to Liu et al. (2025)) and encode information beyond simply cancer type.

Compared to other works investigating multimodal models, we propose a simple yet effective late fusion strategy. We ensemble the predicted outputs of unimodal models as input to the final multimodal model. This further modularizes the modeling of individual modalities (in addition to FM embeddings) and allows the multimodal model to be agnostic to unimodal embeddings. This abstraction simplifies challenges of other fusion approaches. For example, ensuring smaller dimensionality features (such as demographics) are modeled comparably to higher dimensional features (such as expression embeddings) is accomplished implicitly in our framework. This modularity greatly facilitated our experimentation with varying FM embeddings per modality.

To the best of our knowledge, MUSK by Xiang et al. (2025) is the only other work to have explored multimodal survival modeling with pathology reports. While they also utilize LLM summarization to condense their pathology reports, our work differs in key ways. First, unlike the MUSK authors, we do no training of our foundation models and evaluate zero-shot extracted embeddings. Yet their reported multimodal C-index of 0.747 is only comparable to our unimodal results, including naive cancer-type based prediction. Our multimodal fusion of histology and text resulted in C-index = 0.780. We additionally incorporate gene expression and clinical data, alongside histology and text modalities, achieving C-index = 0.795 and further surpassing their dual modality results. Experimentally, due to their language model length limitation, they cannot compare to unsummarized reports as we have. Lastly, their text summarization differs per cancer type, requiring specific, hand-written prompts by an oncologist; while this may focus the most relevant information for a given cancer type, we create a generalizable sum-

marization strategy, applicable to any cancer type, that results in strong downstream predictions.

We further extend our report summarization results to assess the impact that LLM hallucination has on downstream embedding and modeling. While we needed to manually correct 24 of 40 randomly selected summaries, many of these corrections qualitatively involved small details relative to the rest of the summary, e.g. correcting the number of lymph nodes negative for metastases. We found manual correction of LLM summarization hallucinations did not change the risk stratification of the sampled subpopulation, compared to uncorrected summaries. While this was true in our study, we emphasize the importance of this kind of experiment, especially as researchers increasingly rely on LLM generated text.

Limitations. While we aim to do extensive experiments to validate our findings, we note key limitations. First, the small sample size of our hallucination correction experiment potentially limits its generalizability. Indeed, we call on other researchers to do such evaluation under their specific experimental settings for similar work relying on LLM text-generation as an intermediate step. Additionally, we leave variations on dimensionality reduction method and histology embedding models as future work. Lastly, while our work establishes a comprehensive baseline for cancer modeling of TCGA data, our results are currently limited to a single dataset. The primary factor for this limitation is finding data with all studied data modalities, particularly with pathology reports; it is ongoing work to do this external validation.

5. Conclusion

Overall, our study presents a modular framework for multimodal cancer modeling leveraging FM derived embeddings with classical models. We present a quantification of this approach applied to cancer survival prediction over the premier cancer data resource, The Cancer Genome Atlas. We show that multiple data modalities are additive using a simple late fusion technique, leaving the door open for expansion to additional modalities. We present novel results on pathology report-based survival prediction and the effects of LLM hallucinations in summarizing those reports. Altogether, these findings represent an important opportunity for the development, application, and evaluation of FMs towards cancer multi-omics and broader biomedicine.

Acknowledgments

This work was funded in part through the Advanced Research Projects Agency for Health (ARPA-H) under contract 75N92020D00021/5N92023F00002. The views and conclusions contained in this document are those of the authors and should not be interpreted as representing the official policies, either expressed or implied, of the U.S. Government. S.S. is additionally supported by NIH training grant T32GM007281. Overview figure created in BioRender.

References

- Ahtisham Fazeel Abbasi, Muhammad Nabeel Asim, Sheraz Ahmed, Sebastian Vollmer, and Andreas Dengel. Survival prediction landscape: an in-depth systematic literature review on activities, methods, tools, diseases, and databases. *Frontiers in Artificial Intelligence*, 7:1428501, 2024.
- Constantin Ahlmann-Eltze, Wolfgang Huber, and Simon Anders. Deep learning-based predictions of gene perturbation effects do not yet outperform simple linear methods. *BioRxiv*, pages 2024–09, 2024.
- Babak Arjmand, Shayesteh Kokabi Hamidpour, Akram Tayanloo-Beik, Parisa Goodarzi, Hamid Reza Aghayan, Hossein Adibi, and Bagher Larijani. Machine learning: a new prospect in multi-omics data analysis of cancer. *Frontiers in Genetics*, 13:824451, 2022.
- Iz Beltagy, Matthew E Peters, and Arman Cohen. Longformer: The long-document transformer. *arXiv preprint arXiv:2004.05150*, 2020.
- Elliot Bolton, Abhinav Venigalla, Michihiro Yasunaga, David Hall, Betty Xiong, Tony Lee, Roxana Daneshjou, Jonathan Frankle, Percy Liang, Michael Carbin, et al. Biomedlm: A 2.7 b parameter language model trained on biomedical text. *arXiv preprint arXiv:2403.18421*, 2024.
- Rishi Bommasani, Drew A Hudson, Ehsan Adeli, Russ Altman, Simran Arora, Sydney von Arx, Michael S Bernstein, Jeannette Bohg, Antoine Bosselut, Emma Brunskill, et al. On the opportunities and risks of foundation models. *arXiv preprint arXiv:2108.07258*, 2021.
- Glenn W Brier. Verification of forecasts expressed in terms of probability. *Monthly weather review*, 78(1):1–3, 1950.
- Kumardeep Chaudhary, Olivier B Poirion, Liangqun Lu, and Lana X Garmire. Deep learning-based multi-omics integration robustly predicts survival in liver cancer. *Clinical cancer research*, 24(6):1248–1259, 2018.
- Richard J Chen, Tong Ding, Ming Y Lu, Drew FK Williamson, Guillaume Jaume, Andrew H Song, Bowen Chen, Andrew Zhang, Daniel Shao, Muhammad Shaban, et al. Towards a general-purpose foundation model for computational pathology. *Nature Medicine*, 30(3):850–862, 2024.
- Richard J Chen, Tong Ding, Ming Y Lu, Drew FK Williamson, Guillaume Jaume, Bowen Chen, Andrew Zhang, Daniel Shao, Andrew H Song, Muhammad Shaban, et al. Uni2-h-features. <https://huggingface.co/datasets/MahmoodLab/UNI2-h-features>, 2025.
- Travers Ching, Xun Zhu, and Lana X Garmire. Coxnet: an artificial neural network method for prognosis prediction of high-throughput omics data. *PLoS computational biology*, 14(4):e1006076, 2018.
- ENCODE Project Consortium et al. An integrated encyclopedia of dna elements in the human genome. *Nature*, 489(7414):57, 2012.
- David R Cox. Regression models and life-tables. *Journal of the Royal Statistical Society: Series B (Methodological)*, 34(2):187–202, 1972.
- Ziling Fan, Zhangqi Jiang, Hengyu Liang, and Chao Han. Pancancer survival prediction using a deep learning architecture with multimodal representation and integration. *Bioinformatics Advances*, 3(1):vbad006, 2023.
- Maxence Gélard, Guillaume Richard, Thomas Pierrot, and Paul-Henry Cournède. Bulkrnabert: Cancer prognosis from bulk rna-seq based language models. In *Proceedings of the 4th Machine Learning for Health Symposium*, volume 259 of *Proceedings of Machine Learning Research*, pages 384–400. PMLR, 15–16 Dec 2025.
- Aaron Grattafiori, Abhimanyu Dubey, Abhinav Jauhri, Abhinav Pandey, Abhishek Kadian, Ahmad Al-Dahle, Aiesha Letman, Akhil Mathur,

- Alan Schelten, Alex Vaughan, et al. The llama 3 herd of models. *arXiv preprint arXiv:2407.21783*, 2024.
- Yu Gu, Robert Tinn, Hao Cheng, Michael Lucas, Naoto Usuyama, Xiaodong Liu, Tristan Naumann, Jianfeng Gao, and Hoifung Poon. Domain-specific language model pretraining for biomedical natural language processing. *ACM Transactions on Computing for Healthcare (HEALTH)*, 3(1):1–23, 2021.
- Jie Hao, Youngsoon Kim, Tejaswini Mallavarapu, Jung Hun Oh, and Mingon Kang. Interpretable deep neural network for cancer survival analysis by integrating genomic and clinical data. *BMC medical genomics*, 12:1–13, 2019.
- Yaru Hao, Xiao-Yuan Jing, and Qixing Sun. Cancer survival prediction by learning comprehensive deep feature representation for multiple types of genetic data. *BMC bioinformatics*, 24(1):267, 2023.
- Frank E Harrell, Robert M Califf, David B Pryor, Kerry L Lee, and Robert A Rosati. Evaluating the yield of medical tests. *Jama*, 247(18):2543–2546, 1982.
- Allison P Heath, Vincent Ferretti, Stuti Agrawal, Maksim An, James C Angelakos, Renuka Arya, Rosita Bajari, Bilal Baqar, Justin HB Barnowski, Jeffrey Burt, et al. The nci genomic data commons. *Nature genetics*, 53(3):257–262, 2021.
- Lei Huang, Weijiang Yu, Weitao Ma, Weihong Zhong, Zhangyin Feng, Haotian Wang, Qianglong Chen, Weihua Peng, Xiaocheng Feng, Bing Qin, et al. A survey on hallucination in large language models: Principles, taxonomy, challenges, and open questions. *ACM Transactions on Information Systems*, 43(2):1–55, 2025.
- Zhi Huang, Travis S Johnson, Zhi Han, Bryan Helm, Sha Cao, Chi Zhang, Paul Salama, Maher Rizkalla, Christina Y Yu, Jun Cheng, et al. Deep learning-based cancer survival prognosis from rna-seq data: approaches and evaluations. *BMC medical genomics*, 13:1–12, 2020.
- Albert Qiaochu Jiang, Alexandre Sablayrolles, Arthur Mensch, Chris Bamford, Devendra Singh Chaplot, Diego de Las Casas, Florian Bressand, Gianna Lengyel, Guillaume Lample, Lucile Saulnier, L’elio Renard Lavaud, Marie-Anne Lachaux, Pierre Stock, Teven Le Scao, Thibaut Lavril, Thomas Wang, Timothée Lacroix, and William El Sayed. Mistral 7b. *arXiv preprint arXiv:2310.06825*, 2023.
- Georgios A Kaissis, Marcus R Makowski, Daniel Rückert, and Rickmer F Braren. Secure, privacy-preserving and federated machine learning in medical imaging. *Nature Machine Intelligence*, 2(6):305–311, 2020.
- Edward L Kaplan and Paul Meier. Nonparametric estimation from incomplete observations. *Journal of the American statistical association*, 53(282):457–481, 1958.
- Jenna Kefeli and Nicholas Tatonetti. Tcga-reports: A machine-readable pathology report resource for benchmarking text-based ai models. *Patterns*, 5(3), 2024a.
- Jenna Kefeli and Nicholas Tatonetti. Tcga-reports: A machine-readable pathology report resource for benchmarking text-based ai models. *Mendeley Data*, V1, doi: 10.17632/hyg5xkznp1, 2024b.
- Nazish Khalid, Adnan Qayyum, Muhammad Bilal, Ala Al-Fuqaha, and Junaid Qadir. Privacy-preserving artificial intelligence in healthcare: Techniques and applications. *Computers in Biology and Medicine*, 158:106848, 2023.
- Woosuk Kwon, Zhuohan Li, Siyuan Zhuang, Ying Sheng, Lianmin Zheng, Cody Hao Yu, Joseph E. Gonzalez, Hao Zhang, and Ion Stoica. Efficient memory management for large language model serving with pagedattention. In *Proceedings of the ACM SIGOPS 29th Symposium on Operating Systems Principles*, pages 611–626, 2023.
- Yanis Labrak, Adrien Bazoge, Emmanuel Morin, Pierre-Antoine Gourraud, Mickael Rouvier, and Richard Dufour. Biomistral: A collection of open-source pretrained large language models for medical domains. *arXiv preprint arXiv:2402.10373*, 2024.
- Jérôme Lambert and Sylvie Chevret. Summary measure of discrimination in survival models based on cumulative/dynamic time-dependent roc curves. *Statistical methods in medical research*, 25(5):2088–2102, 2016.
- Hong Liu, Haosen Yang, Federica Eduati, Josien PW Pluim, and Mitko Veta. Adaptive prototype learning for multimodal cancer survival analysis. *arXiv preprint arXiv:2503.04643*, 2025.

- Jianfang Liu, Tara Lichtenberg, Katherine A Hoadley, Laila M Poisson, Alexander J Lazar, Andrew D Cherniack, Albert J Kovatich, Christopher C Benz, Douglas A Levine, Adrian V Lee, et al. An integrated tcga pan-cancer clinical data resource to drive high-quality survival outcome analytics. *Cell*, 173(2):400–416, 2018.
- John Lonsdale, Jeffrey Thomas, Mike Salvatore, Rebecca Phillips, Edmund Lo, Saboor Shad, Richard Hasz, Gary Walters, Fernando Garcia, Nancy Young, et al. The genotype-tissue expression (gtex) project. *Nature genetics*, 45(6):580–585, 2013.
- Ming Y Lu, Bowen Chen, Drew FK Williamson, Richard J Chen, Ivy Liang, Tong Ding, Guillaume Jaume, Igor Odintsov, Long Phi Le, Georg Gerber, et al. A visual-language foundation model for computational pathology. *Nature Medicine*, 30(3):863–874, 2024.
- Vidhi Malik, Yogesh Kalakoti, and Durai Sundar. Deep learning assisted multi-omics integration for survival and drug-response prediction in breast cancer. *BMC genomics*, 22:1–11, 2021.
- Michael Moor, Oishi Banerjee, Zahra Shakeri Hossein Abad, Harlan M Krumholz, Jure Leskovec, Eric J Topol, and Pranav Rajpurkar. Foundation models for generalist medical artificial intelligence. *Nature*, 616(7956):259–265, 2023.
- Omri Nayshool, Nitzan Kol, Elisheva Javaski, Ninette Amariglio, and Gideon Rechavi. Surviveai: Long term survival prediction of cancer patients based on somatic rna-seq expression. *Cancer Informatics*, 21:11769351221127875, 2022.
- Karl Pearson. Liii. on lines and planes of closest fit to systems of points in space. *The London, Edinburgh, and Dublin philosophical magazine and journal of science*, 2(11):559–572, 1901.
- Fabian Pedregosa, Gaël Varoquaux, Alexandre Gramfort, Vincent Michel, Bertrand Thirion, Olivier Grisel, Mathieu Blondel, Peter Prettenhofer, Ron Weiss, Vincent Dubourg, et al. Scikit-learn: Machine learning in python. *Journal of machine Learning research*, 12:2825–2830, 2011.
- Sebastian Pölsterl. scikit-survival: A library for time-to-event analysis built on top of scikit-learn. *Journal of Machine Learning Research*, 21(212):1–6, 2020.
- CZI Cell Science Program, Shibli Abdulla, Brian Aevermann, Pedro Assis, Seve Badajoz, Sidney M Bell, Emanuele Bezzi, Batuhan Cakir, Jim Chaffer, Signe Chambers, et al. Cz cellxgene discover: a single-cell data platform for scalable exploration, analysis and modeling of aggregated data. *Nucleic Acids Research*, 53(D1):D886–D900, 2025.
- Yeping Lina Qiu, Hong Zheng, Arnout Devos, Heather Selby, and Olivier Gevaert. A meta-learning approach for genomic survival analysis. *Nature communications*, 11(1):6350, 2020.
- Ricardo Ramirez, Yu-Chiao Chiu, SongYao Zhang, Joshua Ramirez, Yidong Chen, Yufei Huang, and Yu-Fang Jin. Prediction and interpretation of cancer survival using graph convolution neural networks. *Methods*, 192:120–130, 2021.
- Seema Sandeep Redekar, Satishkumar L Varma, and Atanu Bhattacharjee. Identification of key genes associated with survival of glioblastoma multiforme using integrated analysis of tcga datasets. *Computer Methods and Programs in Biomedicine Update*, 2:100051, 2022.
- Yanay Rosen, Yusuf Roohani, Ayush Agarwal, Leon Samotorčan, Tabula Sapiens Consortium, Stephen R Quake, and Jure Leskovec. Universal cell embeddings: A foundation model for cell biology. *bioRxiv*, pages 2023–11, 2023.
- Flavio Sartori, Francesco Codicè, Isabella Caranzano, Cesare Rollo, Giovanni Birolo, Piero Fariselli, and Corrado Pancotti. A comprehensive review of deep learning applications with multi-omics data in cancer research. *Genes*, 16(6):648, 2025.
- Rebecca L Siegel, Tyler B Kratzer, Angela N Giquinto, Hyuna Sung, and Ahmedin Jemal. Cancer statistics, 2025. *Ca*, 75(1):10, 2025.
- Karan Singhal, Shekoofeh Azizi, Tao Tu, S Sara Mahdavi, Jason Wei, Hyung Won Chung, Nathan Scales, Ajay Tanwani, Heather Cole-Lewis, Stephen Pfohl, et al. Large language models encode clinical knowledge. *Nature*, 620(7972):172–180, 2023.
- Bo Sun and Liang Chen. Interpretable deep learning for improving cancer patient survival based on personal transcriptomes. *Scientific Reports*, 13(1):11344, 2023.

- Artur Szalata, Karin Hrovatin, Sören Becker, Alejandro Tejada-Lapuerta, Haotian Cui, Bo Wang, and Fabian J Theis. Transformers in single-cell omics: a review and new perspectives. *Nature methods*, 21(8):1430–1443, 2024.
- Terry Therneau, Cindy Crowson, and Elizabeth Atkinson. Using time dependent covariates and time dependent coefficients in the cox model. *Survival vignettes*, 2(3):1–25, 2017.
- Arun James Thirunavukarasu, Darren Shu Jeng Ting, Kabilan Elangovan, Laura Gutierrez, Ting Fang Tan, and Daniel Shu Wei Ting. Large language models in medicine. *Nature medicine*, 29(8):1930–1940, 2023.
- Katarzyna Tomczak, Patrycja Czerwińska, and Maciej Wiznerowicz. Review the cancer genome atlas (tcga): an immeasurable source of knowledge. *Contemporary Oncology/Współczesna Onkologia*, 2015(1):68–77, 2015.
- Reihaneh Torkzadehmahani, Reza Nasirigerdeh, David B Blumenthal, Tim Kacprowski, Markus List, Julian Matschinske, Julian Spaeth, Nina Kerstin Wenke, and Jan Baumbach. Privacy-preserving artificial intelligence techniques in biomedicine. *Methods of information in medicine*, 61(S 01):e12–e27, 2022.
- Ellery Wulczyn, David F Steiner, Zhaoyang Xu, Apaar Sadhwani, Hongwu Wang, Isabelle Flament-Auvigne, Craig H Mermel, Po-Hsuan Cameron Chen, Yun Liu, and Martin C Stumpe. Deep learning-based survival prediction for multiple cancer types using histopathology images. *PloS one*, 15(6):e0233678, 2020.
- Jinxi Xiang, Xiyue Wang, Xiaoming Zhang, Yinghua Xi, Feyisope Eweje, Yijiang Chen, Yuchen Li, Colin Bergstrom, Matthew Gopaulchan, Ted Kim, et al. A vision–language foundation model for precision oncology. *Nature*, pages 1–10, 2025.
- Zhaochang Yang, Ting Wei, Ying Liang, Xin Yuan, Ruitian Gao, Yujia Xia, Jie Zhou, Yue Zhang, and Zhangsheng Yu. A foundation model for generalizable cancer diagnosis and survival prediction from histopathological images. *Nature Communications*, 16(1):2366, 2025.
- Zhichao Yang, Avijit Mitra, Sunjae Kwon, and Hong Yu. Clinicalmamba: A generative clinical language model on longitudinal clinical notes. *arXiv preprint arXiv:2403.05795*, 2024.
- Xiaohui Zhan, Jun Cheng, Zhi Huang, Zhi Han, Bryan Helm, Xiaowen Liu, Jie Zhang, Tian-Fu Wang, Dong Ni, and Kun Huang. Correlation analysis of histopathology and proteogenomics data for breast cancer. *Molecular & Cellular Proteomics*, 18(8):S37–S51, 2019.
- Zhenyu Zhang, Kyle Hernandez, Jeremiah Savage, Shenglai Li, Dan Miller, Stuti Agrawal, Francisco Ortuno, Louis M Staudt, Allison Heath, and Robert L Grossman. Uniform genomic data analysis in the nci genomic data commons. *Nature communications*, 12(1):1226, 2021.

Appendix A. Manual Correction of Summaries

In our manual correction of generated summaries, we only change factually incorrect information based on information from the original report. We do not add extra information that was not already present in the summary. When the incorrect information cannot be corrected based on the original report, we delete the erroneous text. A salient example of this was when patient age was redacted in the original report. The resulting extracted text thus contained a fragment such as “-year-old patient”, which the summarizing LLM interpreted to mean a 1-year-old patient. Manual verification of the case metadata revealed the patient to be in their 40s, however, because this data was impossible to derive from the original report, we remove the mention of the patient age in the corrected summary. All manual corrections for our experiment were done by a medical student who had completed two years of preclinical medical education. The sampled and corrected summaries are available in our GitHub repository.

For manual correction of summaries, we develop and share a lightweight, interactive tool for comparing unsummarized and summarized reports. The tool allows users to select sections of text in one text box which are automatically highlighted in the other text box. This enables users to quickly and interactively find corresponding information in large spans of text, thus facilitating verification of summaries using the source report. The tool is implemented in pure HTML and JavaScript and runs locally in a web browser, requiring no internet connection to use. We share the tool and a demo video of its use in our GitHub repository.

To better understand the kinds of corrections applied, we qualitatively categorize the 36 correction instances from 24 of 40 total reports in our experiment. We present the correction category counts in Table 11 and provide brief descriptions of these categories here. Descriptor or information mixup is when the summary incorrectly associates information described in multiple, potentially related parts of the report (e.g. swapping tumor vs benign tissue location). Lymph node information in particular was often incorrect, potentially due to the long spans of text that typically describes sentinel lymph node biopsies. A more benign type of error was copy-forward errors from the OCR text extraction process, e.g. NO vs N0 staging. Perhaps the most egregious hallucina-

tion was the inclusion of information not otherwise in the report, for example inferring the indication for the biopsy despite not being included in the original report. Gross description inclusion was considered an error given that we specifically prompted models to exclude gross description; the inclusion of the gross description thus represents conflation of gross and microscopic descriptors by the LLM. Relatedly, there were specific medical phrases used that the model would incorrectly interpret, such as “not otherwise specified”. A specific subtype of this that we identified was with misinterpretation of tumor staging (e.g. a placeholder value “X” to indicate missing or unreported was misinterpreted as the tumor grade; we verified there is no such grade for the given cancer type). Inclusion of patient age was also observed, despite all age being deidentified in the source reports. One summary was grammatically ambiguous. Finally, one correction should not have been included and was an error on the part of the manual corrector; the specific report with the error contained a different OCR error so overall the number of corrected reports remains 24.

Appendix B. Foundation Model Details

For diagnostic slides, we use UNI2-h (Chen et al., 2024) precomputed embeddings. Notably, as UNI2 is a tile/patch-level encoder, we aggregate tile embeddings to a slide-level embedding using simple averaging. For pathology reports or their summaries, we embed text using BioMistral-7B (Labrak et al., 2024) or its source model, Mistral-7B-Instruct-v0.1 (Jiang et al., 2023). We perform embedding inference for these LLMs using vLLM (Kwon et al., 2023). For gene expression data, we experiment with both BulkRNABert (Gélard et al., 2025) and Universal Cell Embedding (UCE) (Rosen et al., 2023). For BulkRNABert, to prevent data leakage, we specifically use the model checkpoint trained over GTEx (Lonsdale et al., 2013) and ENCODE (Consortium et al., 2012) data. For UCE, we use the 33-layer model variant trained over data from CELLxGENE (Program et al., 2025). We make minor modifications to the code repositories for both of these models to enable installation as pip packages and inline data processing. Our modifications are contained in forks of these repositories linked from our main repo.

For the pathology report text modality, we choose BioMistral for its long context length and general

biomedical domain adaptation, as opposed to other long-context LLMs adapted to more specific clinical domains (Yang et al., 2024) unrelated to pathology reports. More specific pathology language models such as CONCH (Lu et al., 2024) or MUSK (Xiang et al., 2025) have been reported, however they are limited by extremely short contexts of 128 and 100 tokens, respectively. In our data, using the Mistral tokenizer (shared by BioMistral), the longest report is 8,184 tokens and the longest summarized report is 1,389 tokens. Despite BioMistral’s domain adaptation with a context length of 2,048, the base Mistral model’s context length of 8,196 and its sliding window attention (Beltagy et al., 2020) enable a theoretical maximum context length that fits all of our pathology reports without truncation. Future work is needed to explore LLMs adapted to the pathology domain at the full context length.

Appendix C. Evaluation of Survival Models

Our primary evaluation metric for our survival models is the concordance index (C-index) (Harrell et al., 1982). For each model, we report the average C-index derived over the test split from 5 cross-validation folds. For model performance by cancer type, we compute the C-index over only cases belonging to each cancer type; as our cross-validation folds are stratified by cancer type and mortality, the number of cases and observed deaths for a given cancer type across folds is approximately equivalent.

While we aim to understand our models’ performance within each cancer type, a consideration with such evaluation is the limited number of potential samples within a given cancer type (see Table 16), particularly when considering cross-validated results. This is an intrinsic limitation of TCGA and public cancer datasets in general, as some cancers are naturally less represented than others; for example, in the case of cholangiocarcinoma (CHOL), prior to data filtering, there are only 51 cases in TCGA. We thus present results in Table 3 over the 8 most prevalent cancer types and in Table 17 over as many cancer types as possible under our experimental setup. Specifically, for certain cancer types with very few observed deaths, as we rely on 5-fold cross-validation for results and due to the multifaceted stratification of our data splits, the observed mortality in specific splits may be extremely limited or is otherwise imperfectly stratified. When there are no observed deaths

in a split (for the given cancer type) or when the observed death is after all other samples are right-censored, it is not possible to derive comparable pairs for computing concordance index. We thus can only present cross-validated results within 27 of the 32 total modeled cancer types. Additionally, while we can compute cross-validated, per-cancer performance for these 27 cancer types, it is important to consider the number of observed events used to compute these results. We thus report the average number of observed deaths and number of samples across test splits in our cross-validation.

To visualize the prognostic capability of our models, we plot averaged risk stratification curves. For a given test split, we binarize the predicted risk about the median into high and low risk groups. For both the low and high risk groups, we compute their Kaplan-Meier curves (Kaplan and Meier, 1958). We repeat this procedure for each cross-validation fold. To compute the average survival curve, we first impute the curves to a shared set of time points before averaging across folds. When visually appropriate, we include shaded regions about the average curves denoting one standard deviation at each time point.

To further validate our findings, we compute two additional evaluation metrics: mean cumulative/dynamic area under the receiver operating characteristic curve (mean AUC^{C,D}) (Lambert and Chevret, 2016) and integrated Brier score (IBS) (Brier, 1950). We specifically compute these metrics over the interval of 1 to 5 years. These boundaries correspond approximately to the 20th and 80th percentiles, respectively, of observation time points within our data.

The only exception to our cross-validated evaluation is in our experiment to manually correct hallucinations in model generated summaries. As cases for this experiment are contained within a single cross-validation fold, we do not report aggregate evaluations for this experiment.

Appendix D. Domain specificity improves cancer modeling

For bulk RNA-seq gene expression modality, we compare our default (BulkRNABert) against Universal Cell Embedding (UCE) (Rosen et al., 2023), a foundation model trained over single cell RNA-seq data. We hypothesized that a single-cell RNA-seq (scRNA-

seq) FM may generalize to the mixed cellular identities of bulk RNA-seq data. While many scRNA-seq FMs exist (Szalata et al., 2024), we chose UCE specifically based on its reported strong performance at extracting multiscale embeddings of cellular biology (Rosen et al., 2023). We find that while UCE derived embeddings do contain some prognostic signal (C-index = 0.637, PCA = 256) which stratifies risk (Figure 5), this is significantly lower compared to BulkRNABert derived embeddings (C-index = 0.753, PCA = 256) and even naive cancer type-based survival (C-index = 0.737, Table 1).

Furthermore, given the strong effects of summarization observed in Figure 3, we test the impact of domain specificity for the text embedding. To isolate the effect of domain adaptation, we compare BioMistral derived embeddings against Mistral-7B-Instruct-v0.1 (Mistral) (Jiang et al., 2023) derived embeddings. We compare BioMistral and Mistral embeddings for both original, unsummarized pathology reports and summarized reports (Figure 6).

We find that for unsummarized reports, embedding FM domain adaptation has a small but appreciable effect on 5-fold cross-validated risk stratification, however it does not change survival prediction performance (Mistral C-index = 0.691 vs BioMistral C-index = 0.691, both PCA = 256). For summarized reports, both risk stratification and risk prediction are equivalent (Mistral C-index = 0.751 vs BioMistral C-index = 0.752). Rather, we recapitulate our previous finding that summarization itself has a greater effect for survival modeling. Given their near equivalence and minor improvement in unsummarized report-based risk stratification, we use BioMistral as our default text embedding model.

Appendix E. Using full embeddings is intractable or leads to overfitting

To test the necessity of dimensionality reduction in our framework, we compare our results to using the full FM-derived embeddings in each unimodal model. The modularity of our framework enables this experiment, however we note that using these full embeddings dramatically increases the computational complexity of the unimodal CoxPH models. When using the text embeddings of size 4096 (see all model embedding sizes in Table 12), a single CoxPH model with a maximum of 100 iterations (the default in the

scikit-survival package) takes an impractical amount of time to train; we stopped the run after 2 hours. The histology embeddings of size 1536 required approximately 11 minutes per model on our hardware. For reference, when using PCA transformation, we can iterate through 7 different PCA dimensionality reduction experiments in 17 minutes on our compute infrastructure, representing 1,085 models in total (each reduction experiment runs 5-fold cross validation where each split has 31 models for all modality combinations i.e. the power set of 5 modalities). Given the full text embedding matrix of approximately 6k train-split samples by 4k covariates, fitting a Cox model over such an input becomes intractable, as the time complexity of training a Cox model is generally $\mathcal{O}(ndp^2)$, where n is the number of samples, d is the number of events, and p is the number of covariates (Therneau et al., 2017). Due to these computational constraints, we are limited to only presenting the comparison to raw embeddings for histology and expression modalities.

Table 13 presents these results comparing the cross validated results for PCA=256 transformed version of embeddings vs the full expression or histology embeddings. We note that the full expression embeddings are size 256 and are thus its results are equivalent to those of the PCA=256 transformed expression embeddings. However, we observe substantial degradation of the unimodal histology model when using the full embedding input. We hypothesize that this is due to overfitting of the histology model to the training data given the high-dimensional histology embedding size of 1536. To verify this, we compare the cross-validated performance on the train vs test splits for both the full expression and full histology embedding models. Indeed, we find greater overfitting of the histology model to the training data when using no dimensionality reduction (Table 14), providing empirical evidence for the inclusion of dimensionality reduction in our framework.

Appendix F. Extended Tables and Figures

Table 4: Average cross-validated integrated Brier score of CoxPH models across varying PCA reductions. Demo: demographics; Canc: cancer type; Expr: BulkRNABert embedded RNA-seq; Hist: UNI2 embedded histology; Text: BioMistral embedded summarized pathology reports; Multimodal: multimodal fusion of all modalities. *Not reduced with PCA.

Modality	PCA Dimension							N/A
	4	8	16	32	64	128	256	
Demo*	-	-	-	-	-	-	-	0.179
Canc*	-	-	-	-	-	-	-	0.155
Expr	0.182	0.177	0.167	0.156	0.154	0.153	0.154	-
Hist	0.182	0.178	0.173	0.165	0.160	0.155	0.153	-
Text	0.185	0.181	0.166	0.159	0.155	0.152	0.153	-
Multimodal	0.152	0.151	0.150	0.145	0.142	0.140	0.140	-

Table 5: Average cross-validated cumulative/dynamic area under the ROC curve of CoxPH models across varying PCA reductions. Demo: demographics; Canc: cancer type; Expr: BulkRNABert embedded RNA-seq; Hist: UNI2 embedded histology; Text: BioMistral embedded summarized pathology reports; Multimodal: multimodal fusion of all modalities. *Not reduced with PCA.

Modality	PCA Dimension							N/A
	4	8	16	32	64	128	256	
Demo*	-	-	-	-	-	-	-	0.650
Canc*	-	-	-	-	-	-	-	0.764
Expr	0.642	0.674	0.728	0.771	0.779	0.783	0.778	-
Hist	0.620	0.647	0.690	0.737	0.760	0.779	0.785	-
Text	0.587	0.634	0.721	0.754	0.773	0.779	0.779	-
Multimodal	0.779	0.783	0.790	0.809	0.820	0.826	0.825	-

Table 6: Late, multimodal fusion of unimodal, FM-based survival models improves survival prediction. For modality combinations with only FM-derived embeddings, average cross-validated C-index of multimodal CoxPH models trained over predicted risk scores from unimodal CoxPH models across varying PCA reductions. Expr: BulkRNABert embedded RNA-seq; Hist: UNI2 embedded histology; Text: BioMistral embedded summarized pathology reports.

Modality	PCA Dimension						
	4	8	16	32	64	128	256
Expr-Hist	0.638	0.665	0.714	0.753	0.765	0.771	0.774
Expr-Text	0.636	0.671	0.724	0.762	0.774	0.779	0.778
Hist-Text	0.606	0.662	0.705	0.746	0.767	0.777	0.780
Expr-Hist-Text	0.644	0.682	0.727	0.765	0.780	0.786	0.788

Table 7: Data modalities encode information beyond cancer type. Addition of other data modalities with cancer type consistently outperforms using cancer type alone. Canc: cancer type; Demo: demographics; Expr: BulkRNABert embedded RNA-seq; Hist: UNI2 embedded histology; Text: BioMistral embedded summarized pathology reports. Average cross-validated results reported using PCA to 256 dimensions for all foundation model derived embeddings.

Combination	C-index
Canc	0.737
Canc-Demo	0.747
Canc-Expr	0.758
Canc-Hist	0.765
Canc-Text	0.761
Canc-Demo-Expr	0.767
Canc-Demo-Hist	0.773
Canc-Demo-Text	0.771
Canc-Expr-Hist	0.774
Canc-Expr-Text	0.776
Canc-Hist-Text	0.779
Canc-Demo-Expr-Hist	0.782
Canc-Demo-Expr-Text	0.784
Canc-Demo-Hist-Text	0.787
Canc-Expr-Hist-Text	0.786
Canc-Demo-Expr-Hist-Text	0.793

Table 8: Hazard ratios of full multimodal fusion model. All modalities confer greater relative risk compared to cancer type. Canc: cancer type; Demo: demographics; Expr: BulkRNABert embedded RNA-seq; Hist: UNI2 embedded histology; Text: BioMistral embedded summarized pathology reports. Results reported using PCA to 256 dimensions for all foundation model derived embeddings.

Split	0	1	2	3	4	Mean
Demo	1.301	1.329	1.340	1.290	1.356	1.323
Canc	0.646	0.640	0.637	0.661	0.625	0.642
Expr	1.899	1.960	1.998	1.959	1.991	1.961
Hist	2.067	2.049	2.052	2.030	2.072	2.054
Text	2.183	2.209	2.193	2.203	2.176	2.193

Table 9: Summarization of pathology reports improves pan-cancer survival prediction. Average cross-validated C-index of models evaluated on subsets of the top 8 most prevalent cancer types in TCGA. All text embedded using BioMistral. Summarized text generated using Llama-3.1-8B-Instruct. Multimodal model incorporates unimodal summarized text model. Results reported using PCA to 256 dimensions for all foundation model derived embeddings.

Modality	Cancer Type (TCGA Project)							
	BRCA	KIRC	UCEC	THCA	LGG	HNSC	LUSC	LUAD
Original	0.612	0.645	0.575	0.593	0.630	0.574	0.540	0.593
Summarized	0.641	0.698	0.723	0.619	0.716	0.582	0.556	0.645
Multimodal	0.720	0.752	0.758	0.787	0.840	0.650	0.626	0.687

Table 10: Pathology report summarization prompt.

Line	Role	Message
1	System	You are a helpful assistant for digital pathology.
2	System	Instructions: Extract and repeat the results of the following pathology report in a single paragraph. Focus on test results, diagnoses and clinical history. Include results of the microscopic description. Omit the gross or macroscopic description. Do not acknowledge this prompt. Do not give additional comments after your final answer.
3	User	(Pathology Report)

Table 11: Categorization of manual corrections for hallucination experiment. Out of 40 sampled reports, 24 reports required manual corrections, totaling 36 specific instances of corrections. These corrections are generally qualitatively minor, though specific error types are more severe than others.

Correction Type	N
descriptor/information mixup	6
incorrect lymph node information	5
copy-forward OCR error	5
made up information not otherwise in report	4
inclusion of gross description	4
misunderstood medical phrase	4
incorrect tumor staging	3
inclusion of patient age	3
grammar clarification	1
manual correction error	1

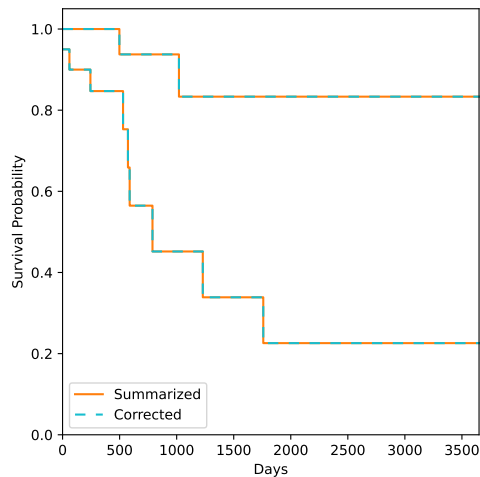


Figure 4: Manual correction of summarized pathology report hallucinations does not impact survival model risk stratification. Embeddings derived with BioMistral. Reports summarized with Llama-3.1-8B-Instruct. Risk stratification from N=40 randomly sampled cases contained within a single test split while preserving observed mortality prevalence.

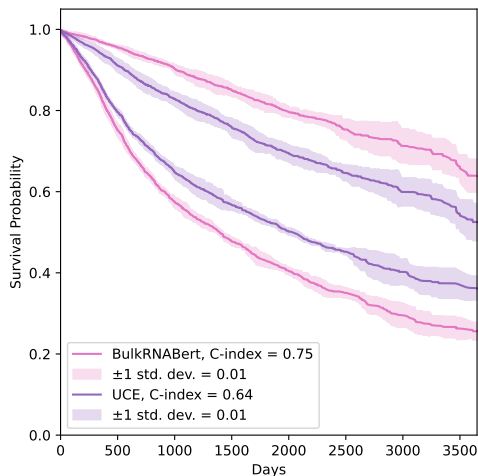


Figure 5: Modality specificity of gene expression embedding model improves survival model risk stratification over unimodal gene expression embeddings. Bulk RNA-seq data embedded with either BulkRNABert or UCE, a single-cell RNA-seq model. Averaged risk stratification from 5-fold cross-validation.

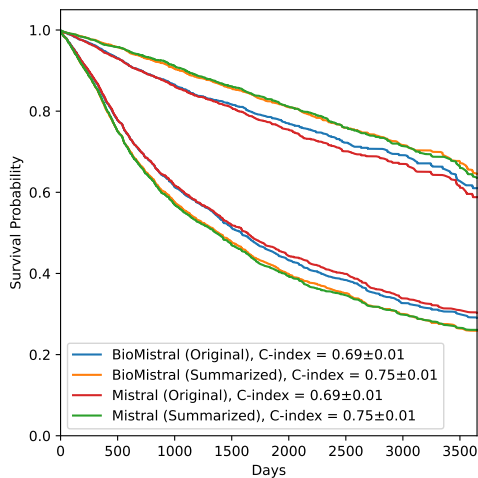


Figure 6: Domain adaptation of text embedding model improves survival model risk stratification over unimodal text embeddings. Embeddings derived with either BioMistral or Mistral-7B-Instruct-v0.1. Reports summarized with Llama-3.1-8B-Instruct. Averaged risk stratification from 5-fold cross-validation.

Table 12: Foundation model embedding dimensionality before PCA reduction. Demo: demographics; Canc: cancer type; Expr: RNA-Seq gene expression; Hist: histology, Text: pathology reports.

Modality	Model	Embedding Size	Is Subsequently PCA Reduced?
Demo	N/A	17	X
Canc	N/A	32	X
Hist	UNI2	1536	✓
Text	BioMistral	4096	✓
Text	Mistral	4096	✓
Expr	BulkRNABert	256	✓
Expr	UCE	1280	✓

Table 13: Average cross-validated C-index of CoxPH models comparing PCA=256 with no dimensionality reduction. Demo: demographics; Canc: cancer type; Expr: BulkRNABert embedded RNA-seq; Hist: UNI2 embedded histology; Text: BioMistral embedded summarized pathology reports; Multimodal: multimodal fusion of all modalities. *Text embedding still PCA reduced to 256d.

	PCA=256	No PCA
Demo	-	0.630
Canc	-	0.737
Expr	0.750	0.750
Hist	0.754	0.700
Text	0.752	-
Multimodal	0.793	0.729*

Table 14: Average cross-validated C-index of CoxPH models comparing train vs test set overfitting/generalization when using full expression or histology embeddings. Expr: BulkRNABert embedded RNA-seq; Hist: UNI2 embedded histology. *Not reduced with PCA.

	Train	Test
Expr*	0.785	0.750
Hist*	0.875	0.700

Table 15: Survival prediction using eight thousand patient cases spanning 32 cancer types from TCGA. All cases have clinical, RNA-seq gene expression, diagnostic histology slides, and pathology reports. Patients split for 5-fold cross-validation, stratified by age bins, sex, race, ethnicity, observed mortality, and cancer type. AA: African American; AIAN: American Indian or Alaska Native; NHPI: Native Hawaiian or Pacific Islander.

	Overall	Cross-Validation Fold				
		0	1	2	3	4
n	7982	1597	1597	1596	1596	1596
Age, mean (SD)	59.8 (14.4)	59.7 (14.4)	59.9 (14.2)	59.9 (14.5)	59.9 (14.3)	59.8 (14.4)
Sex, n (%)						
Female	4192 (52.5)	828 (51.8)	842 (52.7)	845 (52.9)	836 (52.4)	841 (52.7)
Male	3790 (47.5)	769 (48.2)	755 (47.3)	751 (47.1)	760 (47.6)	755 (47.3)
Race, n (%)						
White	6019 (75.4)	1212 (75.9)	1203 (75.3)	1207 (75.6)	1203 (75.4)	1194 (74.8)
Black or AA	794 (9.9)	154 (9.6)	152 (9.5)	165 (10.3)	160 (10.0)	163 (10.2)
Asian	378 (4.7)	72 (4.5)	78 (4.9)	77 (4.8)	78 (4.9)	73 (4.6)
AIAN	20 (0.3)	3 (0.2)	6 (0.4)	2 (0.1)	3 (0.2)	6 (0.4)
NHPI	10 (0.1)	3 (0.2)	2 (0.1)	1 (0.1)	1 (0.1)	3 (0.2)
Unknown	123 (1.5)	24 (1.5)	28 (1.8)	24 (1.5)	21 (1.3)	26 (1.6)
Not Reported	638 (8.0)	129 (8.1)	128 (8.0)	120 (7.5)	130 (8.1)	131 (8.2)
Ethnicity, n (%)						
Not Hispanic/Latino	5983 (75.0)	1197 (75.0)	1197 (75.0)	1197 (75.0)	1192 (74.7)	1200 (75.2)
Hispanic/Latino	309 (3.9)	62 (3.9)	56 (3.5)	59 (3.7)	68 (4.3)	64 (4.0)
Unknown	172 (2.2)	37 (2.3)	39 (2.4)	40 (2.5)	31 (1.9)	25 (1.6)
Not Reported	1518 (19.0)	301 (18.8)	305 (19.1)	300 (18.8)	305 (19.1)	307 (19.2)
Mortality, n (%)						
Alive	5790 (72.5)	1166 (73.0)	1150 (72.0)	1152 (72.2)	1165 (73.0)	1157 (72.5)
Dead	2192 (27.5)	431 (27.0)	447 (28.0)	444 (27.8)	431 (27.0)	439 (27.5)
Survival Time in Days, mean (SD)	1026.6 (964.2)	1048.0 (978.4)	1029.3 (969.7)	1013.8 (956.0)	1021.0 (961.9)	1020.8 (955.5)

Table 16: Eight thousand patient cases span 32 cancer types from TCGA. Cancer types stratified across 5-fold cross-validation splits.

	Overall	Cross-Validation Fold				
		0	1	2	3	4
n	7982	1597	1597	1596	1596	1596
ACC	53 (0.7)	11 (0.7)	9 (0.6)	11 (0.7)	11 (0.7)	11 (0.7)
BLCA	343 (4.3)	67 (4.2)	69 (4.3)	71 (4.4)	67 (4.2)	69 (4.3)
BRCA	982 (12.3)	197 (12.3)	194 (12.1)	197 (12.3)	198 (12.4)	196 (12.3)
CESC	248 (3.1)	49 (3.1)	47 (2.9)	50 (3.1)	50 (3.1)	52 (3.3)
CHOL	33 (0.4)	8 (0.5)	6 (0.4)	5 (0.3)	6 (0.4)	8 (0.5)
COAD	391 (4.9)	78 (4.9)	77 (4.8)	77 (4.8)	81 (5.1)	78 (4.9)
DLBC	43 (0.5)	9 (0.6)	9 (0.6)	8 (0.5)	9 (0.6)	8 (0.5)
ESCA	116 (1.5)	23 (1.4)	26 (1.6)	23 (1.4)	23 (1.4)	21 (1.3)
GBM	142 (1.8)	29 (1.8)	29 (1.8)	28 (1.8)	28 (1.8)	28 (1.8)
HNSC	433 (5.4)	89 (5.6)	88 (5.5)	87 (5.5)	83 (5.2)	86 (5.4)
KICH	65 (0.8)	13 (0.8)	13 (0.8)	13 (0.8)	13 (0.8)	13 (0.8)
KIRC	497 (6.2)	97 (6.1)	100 (6.3)	102 (6.4)	99 (6.2)	99 (6.2)
KIRP	237 (3.0)	48 (3.0)	48 (3.0)	46 (2.9)	48 (3.0)	47 (2.9)
LGG	442 (5.5)	88 (5.5)	90 (5.6)	89 (5.6)	86 (5.4)	89 (5.6)
LIHC	319 (4.0)	62 (3.9)	63 (3.9)	63 (3.9)	67 (4.2)	64 (4.0)
LUAD	411 (5.1)	84 (5.3)	83 (5.2)	82 (5.1)	80 (5.0)	82 (5.1)
LUSC	418 (5.2)	82 (5.1)	82 (5.1)	85 (5.3)	85 (5.3)	84 (5.3)
MESO	66 (0.8)	15 (0.9)	13 (0.8)	12 (0.8)	12 (0.8)	14 (0.9)
OV	42 (0.5)	7 (0.4)	10 (0.6)	9 (0.6)	7 (0.4)	9 (0.6)
PAAD	168 (2.1)	34 (2.1)	32 (2.0)	34 (2.1)	34 (2.1)	34 (2.1)
PCPG	171 (2.1)	34 (2.1)	37 (2.3)	34 (2.1)	34 (2.1)	32 (2.0)
PRAD	326 (4.1)	67 (4.2)	66 (4.1)	66 (4.1)	63 (3.9)	64 (4.0)
READ	144 (1.8)	29 (1.8)	28 (1.8)	29 (1.8)	30 (1.9)	28 (1.8)
SARC	240 (3.0)	49 (3.1)	50 (3.1)	47 (2.9)	47 (2.9)	47 (2.9)
SKCM	94 (1.2)	19 (1.2)	19 (1.2)	17 (1.1)	19 (1.2)	20 (1.3)
STAD	269 (3.4)	52 (3.3)	54 (3.4)	55 (3.4)	54 (3.4)	54 (3.4)
TGCT	87 (1.1)	19 (1.2)	16 (1.0)	15 (0.9)	18 (1.1)	19 (1.2)
THCA	483 (6.1)	96 (6.0)	96 (6.0)	97 (6.1)	98 (6.1)	96 (6.0)
THYM	109 (1.4)	20 (1.3)	21 (1.3)	23 (1.4)	24 (1.5)	21 (1.3)
UCEC	494 (6.2)	99 (6.2)	100 (6.3)	97 (6.1)	99 (6.2)	99 (6.2)
UCS	52 (0.7)	11 (0.7)	10 (0.6)	10 (0.6)	10 (0.6)	11 (0.7)
UVM	64 (0.8)	12 (0.8)	12 (0.8)	14 (0.9)	13 (0.8)	13 (0.8)

Table 17: Multimodal fusion improves survival prediction within given cancer types. Average cross-validated C-index of models evaluated on 27 cancer types in TCGA for which we could compute cross-validated results. Multimodal model used fusion of all unimodal modalities. Results reported using PCA to 256 dimensions for all foundation model derived embeddings. Average cross-validation test fold characteristics provided to demonstrate vanishingly small sample sizes.

	Cancer Type (TCGA Project)									
	BRCA	KIRC	UCEC	THCA	LGG	HNSC	LUSC	LUAD	COAD	
Mean Test Size (N)	196.4	99.4	98.8	96.6	88.4	86.6	83.6	82.2	78.2	
Mean Test Mortality (N)	28.0	33.4	15.8	3.2	20.0	40.6	37.0	29.8	15.8	
Demographics	0.637	0.600	0.593	0.885	0.727	0.525	0.542	0.530	0.563	
RNA-seq	0.573	0.673	0.643	0.619	0.790	0.560	0.579	0.620	0.604	
Histology	0.648	0.685	0.703	0.749	0.753	0.636	0.598	0.617	0.629	
Text	0.641	0.698	0.723	0.619	0.716	0.582	0.556	0.645	0.704	
Multimodal	0.720	0.752	0.758	0.787	0.840	0.650	0.626	0.687	0.718	

	Cancer Type (TCGA Project)									
	BLCA	LIHC	STAD	CESC	SARC	KIRP	PAAD	READ	GBM	
Mean Test Size (N)	68.6	63.8	53.8	49.6	48.0	47.4	33.6	28.8	28.4	
Mean Test Mortality (N)	32.2	20.4	22.6	12.0	17.8	6.6	17.4	4.0	23.4	
Demographics	0.584	0.558	0.525	0.602	0.571	0.498	0.545	0.706	0.596	
RNA-seq	0.594	0.557	0.579	0.670	0.620	0.798	0.634	0.538	0.506	
Histology	0.604	0.590	0.591	0.619	0.590	0.719	0.610	0.587	0.589	
Text	0.576	0.549	0.644	0.603	0.659	0.788	0.616	0.642	0.498	
Multimodal	0.663	0.608	0.676	0.704	0.673	0.846	0.673	0.664	0.570	

	Cancer Type (TCGA Project)									
	ESCA	SKCM	MESO	KICH	UVM	ACC	UCS	OV	CHOL	
Mean Test Size (N)	23.2	18.8	13.2	13.0	12.8	10.6	10.4	8.4	6.6	
Mean Test Mortality (N)	12.2	5.2	11.2	1.8	4.2	3.8	6.8	4.2	3.4	
Demographics	0.579	0.513	0.503	0.615	0.684	0.591	0.631	0.518	0.492	
RNA-seq	0.447	0.617	0.611	0.937	0.652	0.826	0.495	0.653	0.466	
Histology	0.596	0.495	0.643	0.805	0.675	0.713	0.440	0.530	0.437	
Text	0.553	0.619	0.514	0.882	0.530	0.754	0.654	0.498	0.557	
Multimodal	0.576	0.590	0.665	0.937	0.739	0.825	0.628	0.588	0.493	

Compare and Correct Reports

Use this tool to interactively search for text from one report in the other. Simply select text in one text box, either by click/dragging with the cursor or with the arrow/shift keys, and matching text will be highlighted in the other text box. Edit text as necessary. Note that this is not a diff checker. Instead, this tool allows comparison of highly related text that may be substantially different in format, such as comparing original and summarized text.

Source Report	Summarized Report
<p>PREVIOUS DIAGNOSIS INQUIRY REPORT DATE: 2. SEX: M. BIRTHDATE: ADM DATE: OPER DATE: PROCEDURE: APMI. ADDITIONAL REPORT FOLLOWING ADDITIONAL SECTIONS AND IMMUNOHISTOCHEMISTRY: Please see diagnosis below. PROCEDURE: APDX. 1. Adrenal gland, left, resection: Adrenocortical carcinoma, low-grade by mitotic activity, with capsular and vascular invasion. Ki-67 proliferation marker shows a proliferation rate above that typically found in benign tumors. See COMMENT. COMMENT: This adrenocortical neoplasm has a very low mitotic activity as assessed by counting of mitotic figures. The Ki-67 proliferation marker shows a proliferation rate that is consistent with the diagnosis of low grade adrenocortical carcinoma. In addition, research immunostains show a similar proliferation rate using topoisomerase 2-alpha. Furthermore, the tumor shows diffuse nuclear immunoreactivity for cyclin E which is also consistent with a diagnosis of carcinoma. (These research stains are not performed by a certified Tab and therefore are not billed to the patient, signing staff pathologist, have personally examined and interpreted the stains from this case. *This test was developed and its performance characteristics determined by the. Inical Immunoperoxidase Laboratory. It has not been, cleared or approved by the U.S. Food and Drug Administration. (The FDA has determined that such clearance is not necessary. This test is used for. PREVIOUS DIAGNOSIS INQUIRY REPORT DATE: 3. SEX: M. BIRTHDATE: PAT TYP. ADM DATE: OPER DATE: clinical purposes. It should not be regarded as investigational or for. research. This laboratory is certified under the Clinical Laboratory Improvement Amendments of 1988 [CLIA] as qualified to perform high complexity testing). OPER DATE: PROCEDURE: SPHS. year-old male with left adrenal mas. PROCEDURE: SPGD. 1. "Left adrenal" Received fresh in a medium container is a 110 gram adrenal with a scant amount of attached yellow adipose, 7.9 x 6.2 x 5.7 cm. The cut surface is remarkable for a 6.2 x 5.3 x 6.0 cm, tan-brown, faintly-nodular, soft, well-circumscribed tumor. The tumor has focal areas of bright-yellow necrosis occupying approximately 15% of the cut surface. Tumor abuts the margin. A 1.1 x 2.3 x 0.5 cm segments of normal adrenal gland is present. NO other abnormalities are noted. Photographs have been taken. 1A&B. Tumor to normal. 1C-G. Tumor to capsule. 1H. Normal adrenal. PROCEDURE: SPDX. 1. Adrenal gland, left, resection: Adrenocortical carcinoma, low-grade by mitotic activity, with capsular invasion. Additional report pending additional sections and immunohistochemistry, the signing staff pathologist, have personally examined and interpreted the slides from this case. Criteria in 12/22/12.</p>	<p>A male patient underwent a left adrenal gland resection due to a left adrenal mass. The microscopic description of the tumor shows a 6.2 x 5.3 x 6.0 cm, tan-brown, faintly-nodular, soft, well-circumscribed tumor with focal areas of bright-yellow necrosis occupying approximately 15% of the cut surface. The tumor abuts the margin and has a 1.1 x 2.3 x 0.5 cm segment of normal adrenal gland present. The tumor is diagnosed as an adrenocortical carcinoma, low-grade by mitotic activity, with capsular and vascular invasion. The Ki-67 proliferation marker shows a proliferation rate above that typically found in benign tumors, and research immunostains show a similar proliferation rate using topoisomerase 2-alpha and diffuse nuclear immunoreactivity for cyclin E, which is consistent with a diagnosis of carcinoma.</p>

Figure 7: Manual review of generated summaries is facilitated by our simple comparison utility. Users dynamically highlight text between reports and can edit as needed. This is more powerful than traditional diff-checkers as summarized reports often fix typos or contain semantically similar text that is not an exact string match. The tool is implemented in pure HTML/JavaScript and does not require an internet connection to use.